Phenomenon of Conversion Polymorphism in Bi-Containing Metastable Perovskites

Dmitry D. Khalyavin, [a] Andrei N. Salak, [b] Elena L. Fertman, [c] Oleksandr V. Kotlyar, [c] Edwin Eardley, [d] Nikolai M. Olekhnovich, [e] Anatoli V. Pushkarev, [e] Yury V. Radyush, [e] Alexey V. Fedorchenko, [c] Vladimir A. Desnenko, [c] Pascal Manuel, [a] Lei Ding, [a] Erik Čižmár, [f] Alexander Feher [f]

[a]*ISIS Facility, Rutherford Appleton Laboratory, Chilton, OX11 0QX Didcot, United Kingdom*
[b]*Department of Materials and Ceramic Engineering and CICECO – Aveiro Institute of Materials, University of Aveiro, 3810-193 Aveiro, Portugal*
[c]*B. Verkin Institute for Low Temperature Physics and Engineering of NAS of Ukraine, 61103 Kharkov, Ukraine*
[d]*Element Six UK Ltd., Global Innovation Centre, Harwell Oxford, OX11 0QR Didcot, United Kingdom*
[e]*Scientific-Practical Materials Research Centre of NAS of Belarus, 220072 Minsk, Belarus*
[f]*Faculty of Science, P. J. Šafárik University in Košice, 04154 Košice, Slovakia*

E-mail addresses:
dmitry.khalyavin@stfc.ac.uk (Dr. Dmitry D. Khalyavin)
salak@ua.pt (Dr. Andrei N. Salak)

1. Experimental Section

Polycrystalline samples of the $BiFe_{1-y}Sc_yO_3$ series with y=0.2, 0.25, 0.3, 0.35, 0.4, 0.45, 0.5, 0.55, 0.6, 0.7, 0.8 and 1.0 were prepared under high-pressure and high-temperature conditions, using high-purity Bi_2O_3, Fe_2O_3, and Sc_2O_3 as starting reagents. The oxides were mixed in the stoichiometric ratio, ball-milled in ethanol, dried, and pressed into pellets. The pellets were heated in a closed alumina crucible at 1040 K for 10 min followed by quenching in air. The obtained material served as a precursor for the high pressure synthesis. High pressure was generated using a hydraulic anvil press DO-138A (with a press capacity of 6300 kN) equipped with a Bridgman-type apparatus. The samples were synthesized at 6 GPa and 1370–1470 K for 1–2 min. For further analyses, the obtained ceramics were reduced to powders.

In order to estimate the stability limits of the perovskite phases prepared under high pressure, the obtained ceramic samples were annealed at temperatures between 870 and 1120 K with a 50 K step for the compositions with y<0.50 and between 770 and 970 K with a 20 K step for the compositions with y≥0.50. The samples were put in a furnace heated to the certain temperature and quenched in air after a 2-h dwell. The annealing temperature was increased until reflections attributed to the cubic sillenite-type phase based on γ-Bi_2O_3 were detected in the XRD patterns.[1] The thermal stability limit was defined as the temperature which is 50 K lower than that when the sillenite-type phase appears.

In situ XRD measurements were conducted in an Anton Paar high-temperature chamber (HTK 16N) in a temperature range between 300 and 870-920 K (depending on composition) with a step of 20 K for both heating and cooling. A dwell time before the XRD data collecting at each temperature point was 30 min.

Neutron powder diffraction data were collected at the ISIS pulsed neutron and muon facility of the Rutherford Appleton Laboratory (UK) on the WISH diffractometer located at the second target station.[2] The sample was loaded into a cylindrical 3-mm-diameter vanadium can and measured in a temperature range of 1.5–300 K. Crystal and magnetic structures solution and refinement were performed using the FULLPROF program[3] and were assisted with group theoretical calculations using ISOTROPY and ISODISTORT software.[4,5] Magnetization measurements were done using a superconducting quantum interference device (SQUID) magnetometer (Quantum Design MPMS).

2. Stability of the high-pressure prepared BiFe$_{1-y}$Sc$_y$O$_3$ perovskites at ambient pressure

The stability limit temperature of perovskite phase in the BiFe$_{1-y}$Sc$_y$O$_3$ system was found to depend on the scandium content and decreases as y is increased (Table S1).

The phases remained in the high-pressure prepared samples after annealing at temperatures by 100 K above their stability limits were identified to be the rhombohedral perovskite phase and the cubic sillenite-type one (Figure S1).

Table S1. Temperatures of the thermal stability limit of the perovskite phases in the BiFe$_{1-y}$Sc$_y$O$_3$ system.

Composition	Temperature
$y<0.15$	stable until melting
$0.20 \leq y \leq 0.25$	970 K
$0.30 \leq y < 0.50$	920 K
$0.50 \leq y \leq 0.70$	870 K
$0.70 < y \leq 1.00$	850 K
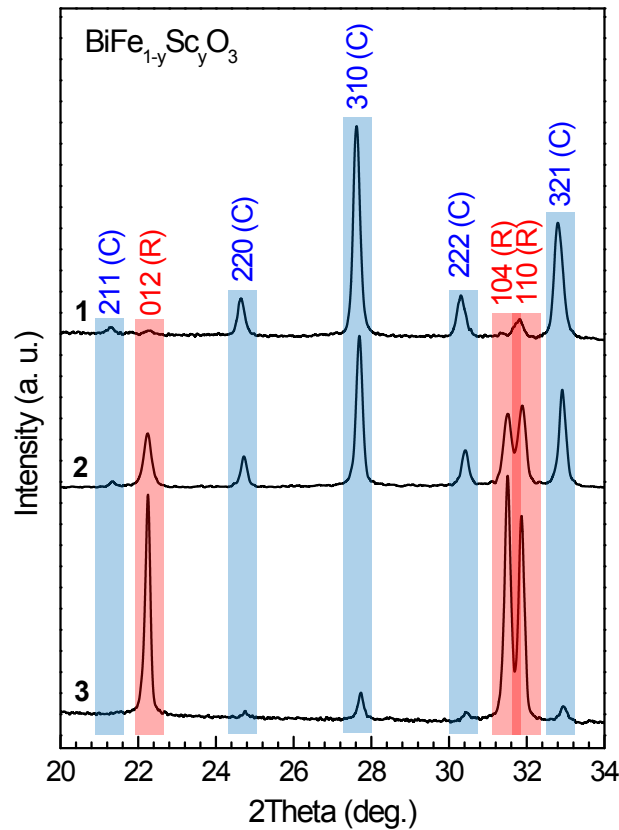
Fig. S1 The XRD patterns of the BiFe$_{1-y}$Sc$_y$O$_3$ samples synthesized at 6 GPa and 1370-1470 K and then annealed in air at temperatures above the stability limits of their metastable perovskite phases: (1) the monoclinic $C/2c$ in the sample with $y=0.70$, (2) the orthorhombic $Pnma$ in the sample with $y=0.45$ and (3) the rhombohedral $R3c$ in the samples with $y=0.20$. The diffraction reflections assigned to the rhombohedral ($R3c$) perovskite phase and to the cubic ($I23$) phase based on γ-Bi$_2$O$_3$ marked as (R) and (C), respectively.

3. *In situ* T-XRD study of the annealing behaviour of the high-pressure synthesized BiFe$_{1-y}$Sc$_y$O$_3$ samples
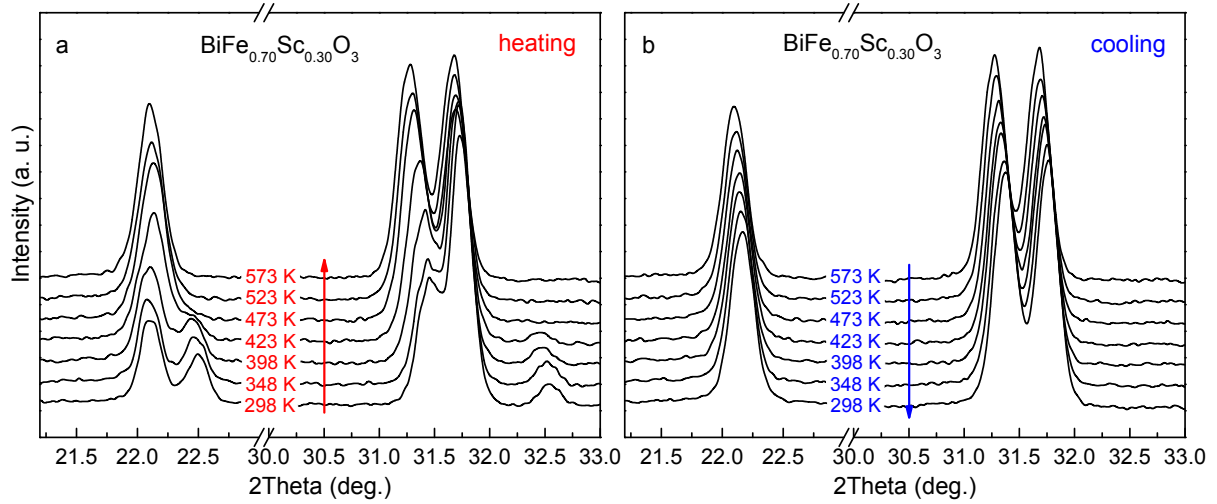
Fig. S2 The most representative ranges of the XRD patterns of the as-prepared BiFe$_{0.70}$Sc$_{0.30}$O$_3$ perovskite at the first thermal cycle: (a) upon heating to 923 K and (b) upon cooling to room temperature. The structural phases at room temperature before and after the annealing are *Pnma* (I) and *R3c*, respectively.
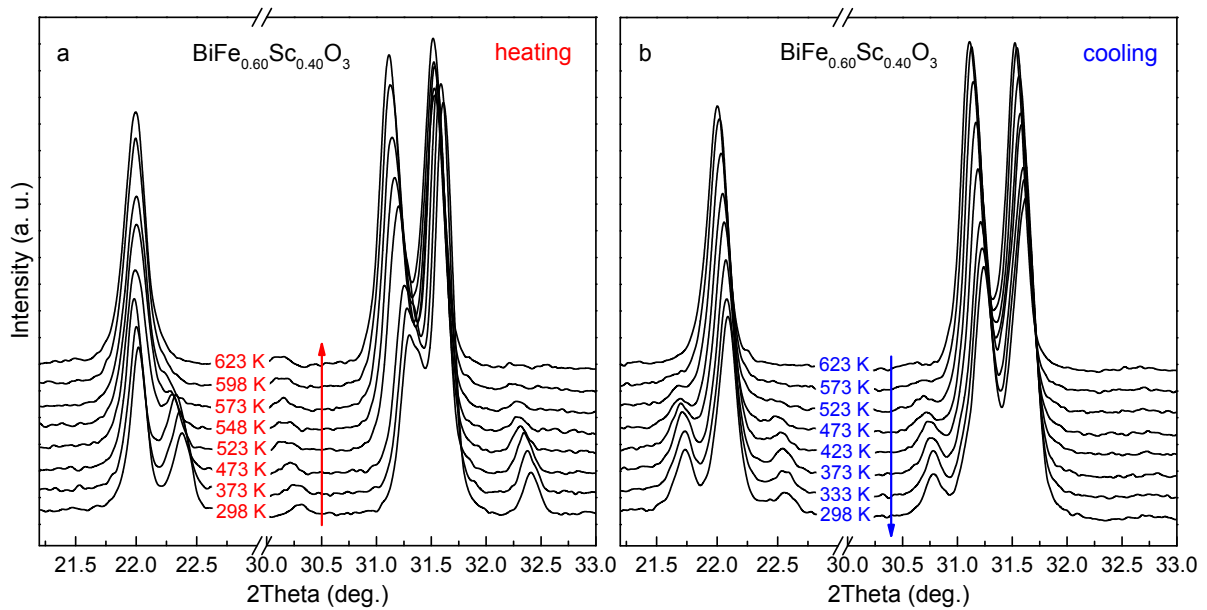
Fig. S3 The most representative ranges of the XRD patterns of the as-prepared BiFe$_{0.60}$Sc$_{0.40}$O$_3$ perovskite at the first thermal cycle: (a) upon heating to 923 K and (b) upon cooling to room temperature. The structural phases at room temperature before and after the annealing are *Pnma* (I) and a mixture *R3c* + *Ima*2, respectively.
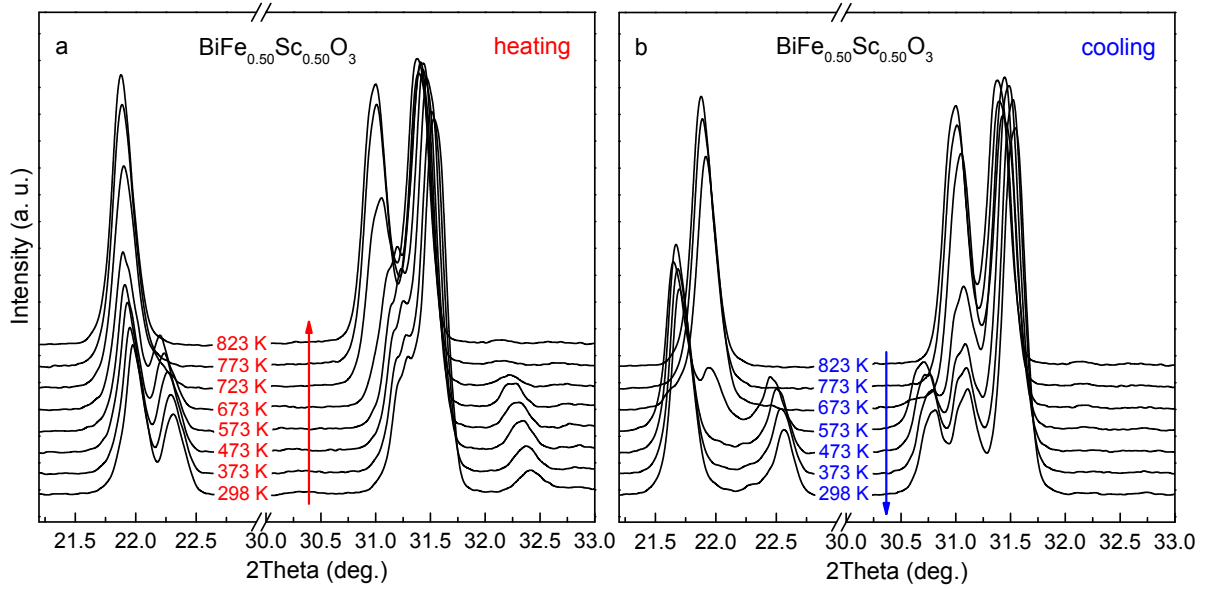
Fig. S4 The most representative ranges of the XRD patterns of the as-prepared $BiFe_{0.50}Sc_{0.50}O_3$ perovskite at the first thermal cycle: (a) on heating up to 873 K and (b) on cooling down to room temperature. The structural phases at room temperature before and after the annealing are *Pnma* (I) and *Ima*2, respectively.
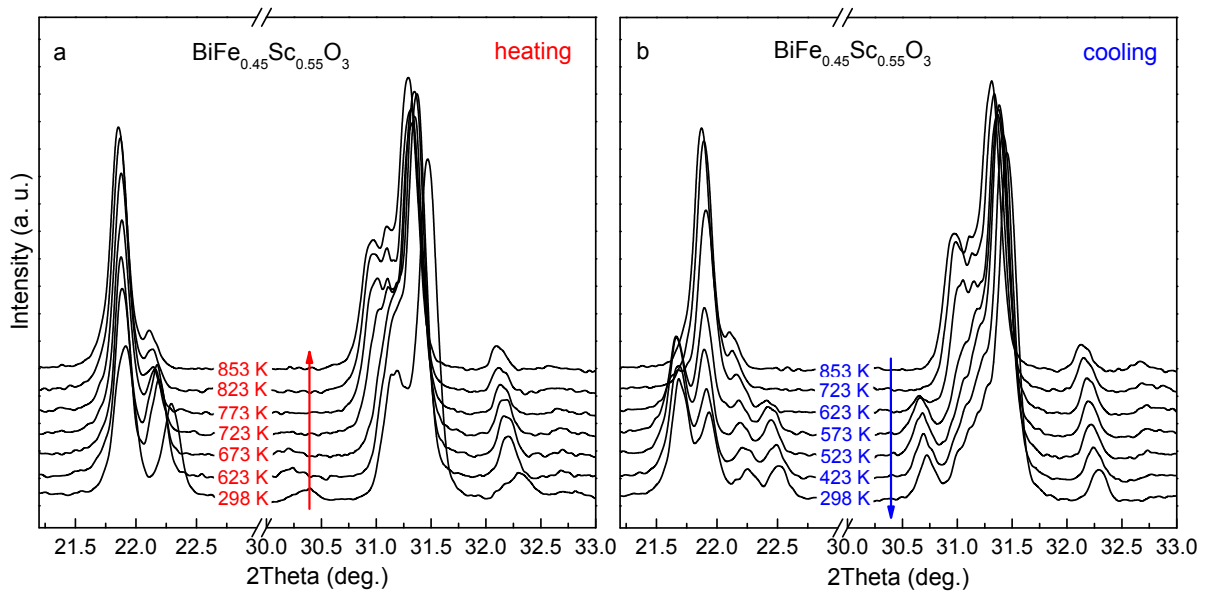
Fig. S5 The most representative ranges of the XRD patterns of the as-prepared $BiFe_{0.45}Sc_{0.55}O_3$ perovskite at the first thermal cycle: (a) upon heating to 853 K and (b) upon cooling to room temperature. The structural phases at room temperature before and after the annealing are *Pnma* (I) and a mixture *Pnma* (I) + *Ima*2, respectively.

It was attempted to complete the irreversible transitions in the $BiFe_{1-y}Sc_yO_3$ samples, in which the annealing resulted in the phase mixture, namely *R*3*c* + *Ima*2 (*y*=0.40 and 0.45) and *Pnma* (I) + *Ima*2 (*y*=0.55). Neither increase in the annealing time nor additional thermal cycles have been found to result in any considerable change of the phase ratio in the phase mixture.
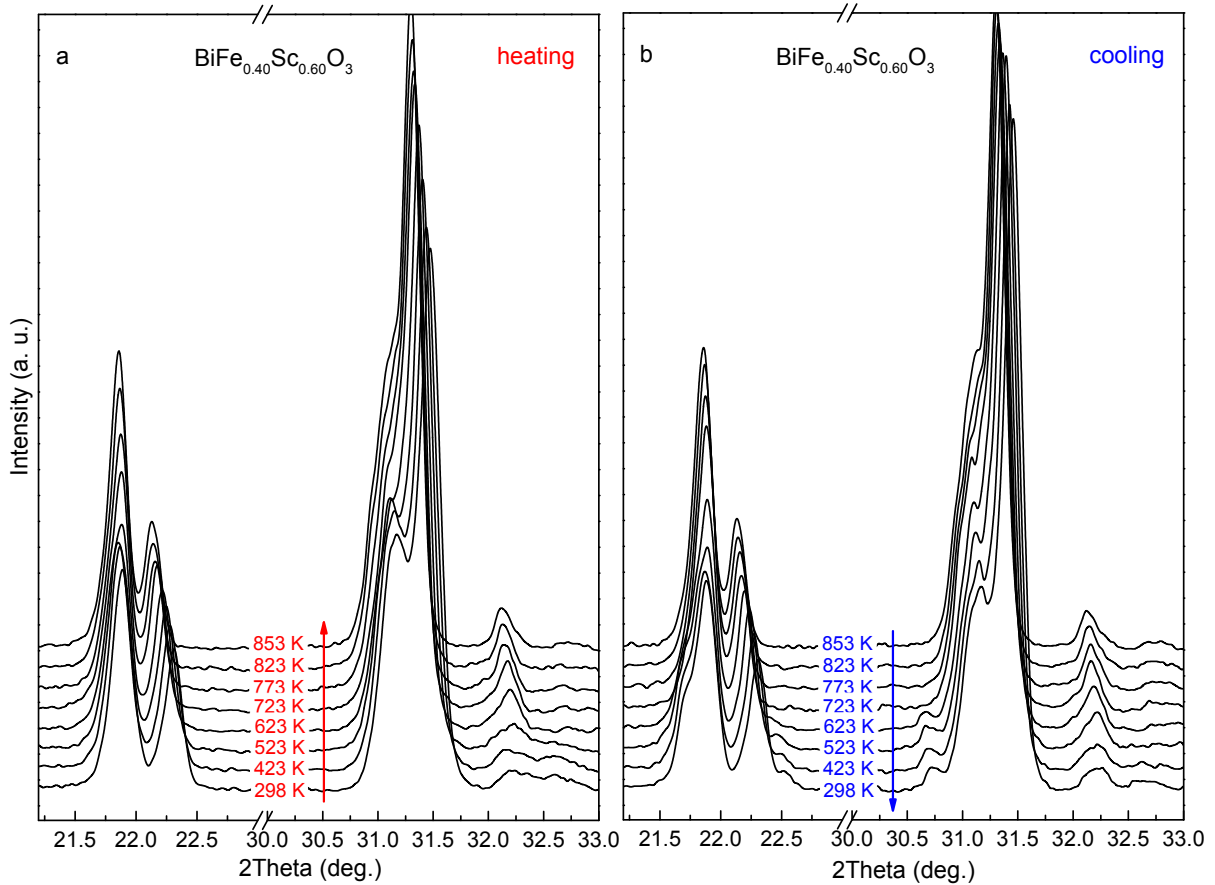
Fig. S6 The most representative ranges of the XRD patterns of the as-prepared $BiFe_{0.40}Sc_{0.60}O_3$ perovskite at the first and the following thermal cycles: (a) upon heating to 853 K and (b) upon cooling to room temperature. The structural phase at room temperature before and after the annealing is the same *Pnma* (I).
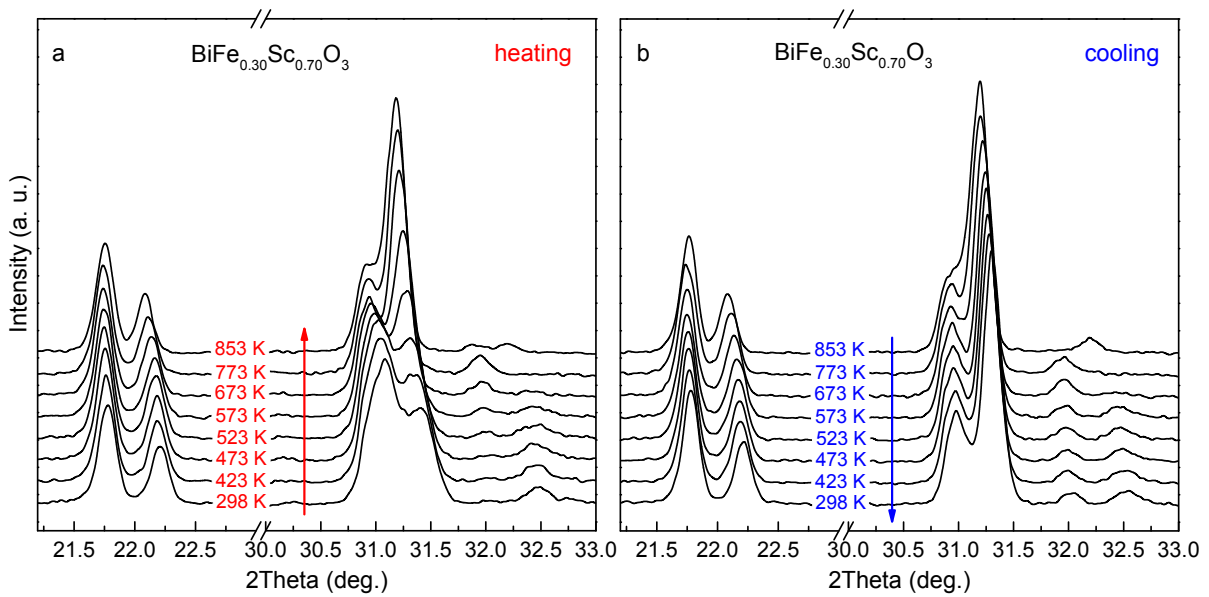
Fig. S7 The most representative ranges of the XRD patterns of the as-prepared $BiFe_{0.30}Sc_{0.70}O_3$ perovskite at the first thermal cycle: (a) upon heating to 853 K and (b) upon cooling to room temperature. The structural phases at room temperature before and after the annealing are *C2/c* and *Pnma* (II), respectively.
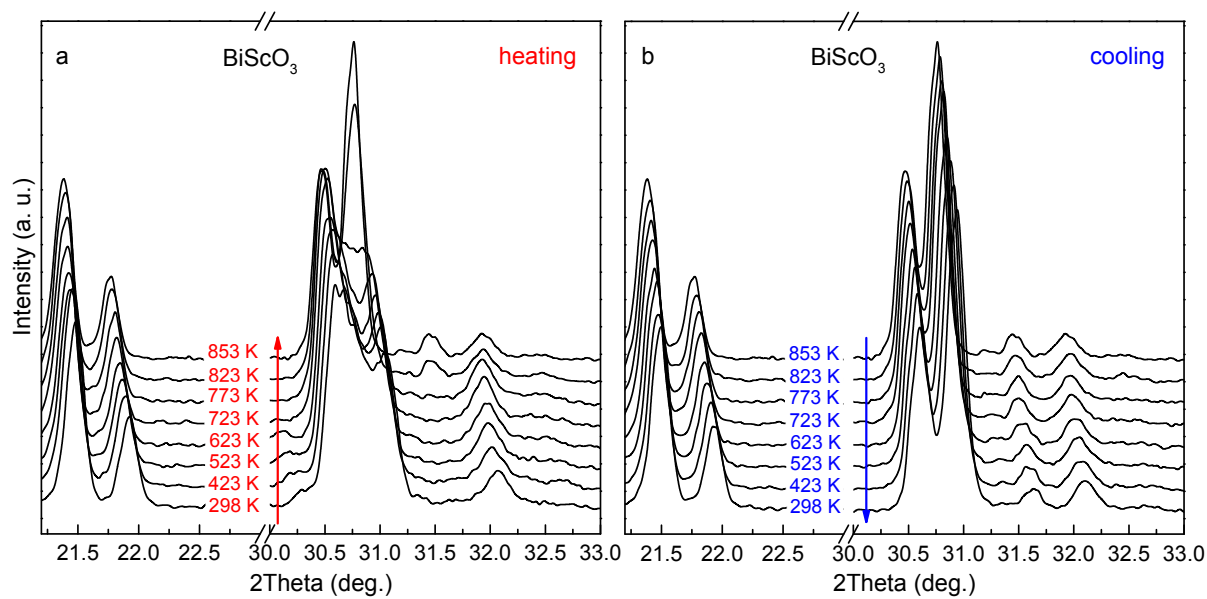
Fig. S8 The most representative ranges of the XRD patterns of the as-prepared BiScO$_3$ perovskite at the first thermal cycle: (a) upon heating to 853 K and (b) upon cooling to room temperature. The structural phases at room temperature before and after the annealing are *C*2/*c* and *Pnma* (II), respectively.

4. Crystal and magnetic structures of $BiFe_{0.7}Sc_{0.3}O_3$

Orthorhombic Pnma polymorph Crystal structure of the as-prepared $BiFe_{0.7}Sc_{0.3}O_3$ perovskite was refined from neutron diffraction data in *Pnma* space group using the model reported in Ref.[6] for $BiFe_{0.5}Sc_{0.5}O_3$. The structural parameters are summarized in Table S2 and the fitting quality is demonstrated in Figure S9. The refinement also included magnetic ordering with *G*-type spin configuration and the moment direction along the *b*-axis (*Pn'm'a* magnetic space group), identical to the magnetic structure of the as-prepared $BiFe_{0.5}Sc_{0.5}O_3$ perovskite.[6] The value of the ordered magnetic moment at *T*= 5 K was refined to be 3.4(1) μ_B per Fe/Sc sites (two independent Fe/Sc sites were constrained to have equal ordered moments). Magnetic ordering persisted up to temperatures, where the irreversible transformation to the polar *R3c* polymorph took place (~380 K). This prevented us to determine the transition temperature to paramagnetic state for this orthorhombic *Pnma* polymorph.
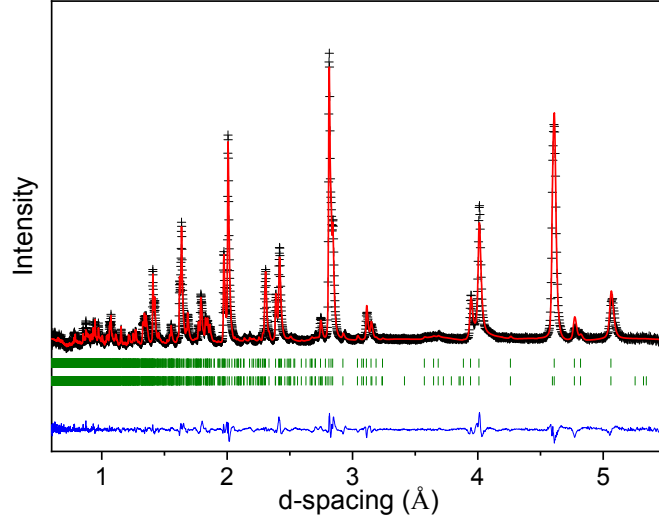
Fig. S9 Rietveld refinement of the neutron diffraction data of the orthorhombic polymorph of $BiFe_{0.7}Sc_{0.3}O_3$, collected at *T*= 5 K (R_{Bragg}=6.61%).

Table S2. Atomic coordinates and thermal parameters for the as-prepared $BiFe_{0.7}Sc_{0.3}O_3$ sample at *T*= 5 K, refined in the *Pnma* space group with the basis vectors related to the parent cubic cell as $a_o=a_p+c_p$, $b_o=4b_p$, $c_o=-2a_c+2c_p$ and origin at ($a_p/2+3b_p/2$). Unit cell parameters: a_o=5.6605(2)Å, b_o=15.7832(5)Å and c_o=11.3751(4)Å. $R_{Bragg(neutr)}$=6.61%

Atom	Site	x	y	z	B
Bi1	4*c*	0.170(4)	0.25	0.624(2)	1.8(2)
Bi2	4*c*	0.293(4)	0.25	0.134(2)	1.8(2)
Bi3	8*d*	0.287(2)	-0.0117(7)	0.121(1)	1.8(2)
Fe/Sc1	8*d*	0.766(2)	0.6222(6)	0.123(1)	1.6(1)
Fe/Sc2	8*d*	0.756(2)	0.1344(5)	0.121(1)	1.6(1)
O1	8*d*	0.038(2)	0.6142(9)	0.011(2)	1.4(1)
O2	8*d*	0.022(3)	0.5920(9)	0.507(2)	1.4(1)
O3	8*d*	0.532(4)	0.656(1)	0.763(2)	1.4(1)
O4	8*d*	0.554(3)	0.137(1)	0.774(2)	1.4(1)
O5	4*c*	0.816(5)	0.25	0.605(3)	1.4(1)
O6	4*c*	0.684(5)	0.25	0.091(3)	1.4(1)
O7	8*d*	0.727(2)	-0.0020(11)	0.167(1)	1.4(1)

Polar R3c polymorph Structural parameters for the annealed polymorph of $BiFe_{0.7}Sc_{0.3}O_3$, refined using neutron diffraction data collected at T= 5 K, are summarized in Table S3 and the fitting quality is demonstrated in Figure 1 of the main text. The refinement included magnetic ordering with *G*-type spin configuration and the moment direction along the *c*-axis (*R3c* magnetic space group). The value of the ordered magnetic moment at T= 5 K was refined to be 2.8(1) μ_B per Fe/Sc site. Transition temperature to paramagnetic state is T_N~410 K as follows from temperature dependence of the magnetic reflection shown in Figure S9.

Table S3 Atomic coordinates and thermal parameters for the annealed $BiFe_{0.7}Sc_{0.3}O_3$ sample at T=5 K, refined in the *R3c* space group with the basis vectors related to the parent cubic cell as $\boldsymbol{a_R}=\boldsymbol{-a_p}+\boldsymbol{b_c}$, $\boldsymbol{b_R}=\boldsymbol{-b_p}+\boldsymbol{c_p}$, $\boldsymbol{c_m}=2\boldsymbol{a_c}+2\boldsymbol{b_p}+2\boldsymbol{c_p}$ and origin at (0,0,0). Unit cell parameters: a_R=5.6295(1)Å, and c_R=14.0273(4) Å. $R_{Bragg(neutr)}$=5.34%

Atom	Site	x	y	z	B
Bi	6a	0	0	0.2791(2)	1.40(8)
Fe/Sc	6a	0	0	0	1.55(7)
O	18b	0.6466(5)	0.8915(5)	0.0646(3)	1.23(6)
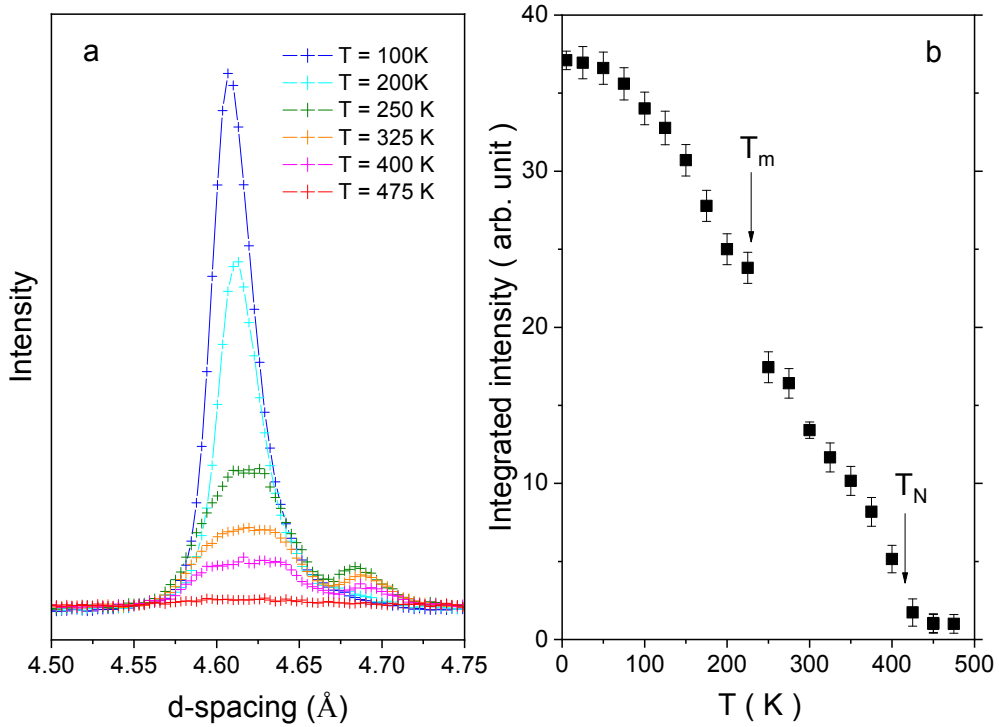
Fig. S10 Neutron diffraction patterns at a vicinity of the strongest magnetic reflection (1/2,1/2,1/2), referring to the pseudocubic unit cell, measured at different temperatures (a). Integrated intensity of this reflection as a function of temperature (b).

5. Crystal structure of $BiScO_3$

Monoclinic C2/c polymorph. Crystal structure of the as-papered sample of $BiScO_3$ has been refined in the monoclinic $C2/c$ space group reported by Belik *et al.*[7] using the neutron diffraction data collected at room temperature (see Fig. S10). The atomic coordinates and the mode decomposition details of the structure are summarized in Table S4 and Table S5, respectively.
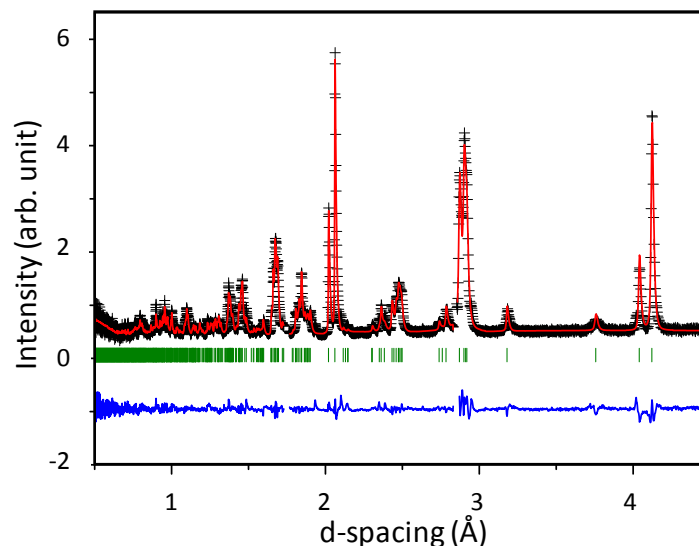
Fig. S11 Rietveld refinement of the neutron diffraction data of the monoclinic $C2/c$ polymorph of $BiScO_3$, collected at room temperature (R_{Bragg}=6.66%).

Table S4. Atomic coordinates and thermal parameters for the as-prepared $BiScO_3$ sample at T=300 K, refined in the $C2/c$ space group with the basis vectors related to the parent cubic cell as $a_m=2a_p+b_c+c_p$, $b_m=4b_p$, $c_m=-2a_c+b_p+c_p$ and origin at $(a_p/2+c_p/2)$. Unit cell parameters: a_m=9.9049(4)Å, b_m=5.8234(3)Å, c_m=10.0398(4)Å and β=108.30(3). $R_{Bragg(neutr)}$=6.66%

Atom	Site	x	y	z	B
Bi1	8f	0.1332(5)	0.1881(6)	0.1286(7)	2.0(1)
Sc1	4e	0	0.2427(6)	0.75	2.24(8)
Sc2	4d	0.25	0.25	0.5	2.24(8)
O1	8f	0.0743(6)	0.201(1)	0.5762(7)	2.7(2)
O2	8f	0.1619(6)	0.529(1)	0.3647(7)	1.8(2)
O3	8f	0.3543(6)	0.530(1)	0.1631(6)	1.3(2)

Table S5. Decomposition of the $C2/c$ structure of the as-prepared BiScO$_3$ sample in respect of the symmetrized displacive modes of the parent cubic $Pm\bar{3}m$ perovskite structure (a_p=4.09610Å, Bi 1b(1/2,1/2,1/2), Sc 1a(0,0,0) and O 3d(1/2,0,0)). The column "Irrep ($\boldsymbol{k}$)" shows the irreducible representation of the $Pm\bar{3}m$ space group and the arms of the wave vector star involved (for the propagation vectors inside the Brillouin zone, –$\boldsymbol{k}$ are not displayed). The column "Order parameter" lists the projections of the reducible order parameter onto the corresponding irreducible subspace (the same symbol in different positions indicates equal order parameter components). The column "Amplitude" displays amplitudes (in Å) of the displacive modes. The column "Site irrep" shows the corresponding point-group symmetry irrep of the local Wyckoff position and the order parameter component (in brackets).

Irrep ($\boldsymbol{k}$)	Order parameter	Site irrep	Amplitude
	Strains		
Γ_1^+ (0,0,0)	(a), $e_{xx}+e_{yy}+e_{zz}$		0.00012
Γ_3^+ (0,0,0)	$(a,\sqrt{3}a)$, $-e_{yy}-e_{zz}+2e_{xx}$		-0.01639
Γ_5^+ (0,0,0)	(a,b,a), $e_{xy}+e_{xz}$	(a)	-0.01005
	e_{yz}	(b)	0.00208
	Bi-displacement		
Λ_3 (-1/4,1/4,1/4)	$(0,0,0,0;a,-a,-1/\sqrt{3}a,-1/\sqrt{3}a;0,0,0,0;0,0,0,0)$	$T_{1u}(a)$	0.71714
R_5^+ (1/2,1/2,1/2)	(a,b,a)	$T_{1u}(a)$	0.13671
		$T_{1u}(b)$	0.07537
	Sc-displacement		
Λ_3 (-1/4,1/4,1/4)	$(0,0,0,0;a,-a,-1/\sqrt{3}a,-1/\sqrt{3}a;0,0,0,0;0,0,0,0)$	$T_{1u}(a)$	0.05980
	O-displacement		
Λ_2 (-1/4,1/4,1/4)	$(0,0;0,a;0,0;0,0)$	$E_u(a)$	0.06053
Λ_3 (-1/4,1/4,1/4)	$(0,0,0,0;a,-a,-1/\sqrt{3}a,-1/\sqrt{3}a;0,0,0,0;0,0,0,0)$	$A_{2u}(a)$	0.08631
		$E_u(a)$	0.651052
		$E_u(a)$	-0.51652
R_1^+ (1/2,1/2,1/2)	(a)	$A_{2u}(a)$	-0.02696
R_3^+ (1/2,1/2,1/2)	$(a,\sqrt{3}a)$	$A_{2u}(a)$	0.05719
R_4^+ (1/2,1/2,1/2)	$(a,0,-a)$	$E_u(a)$	1.68350
R_5^+ (1/2,1/2,1/2)	(a,b,a)	$E_u(a)$	-0.05325
		$E_u(b)$	-0.05156

Orthorhombic Pnma polymorph Crystal structure of the annealed sample of $BiScO_3$ was determined by a joint refinement of the neutron and X-ray diffraction data combined with a comprehensive symmetry analysis. The main reflections on the both diffraction patterns can be indexed using the orthorhombic cell ($\sqrt{2}a_p \times 2\sqrt{2}a_p \times 2a_p$) characteristic of the $PbZrO_3$ structural type (space group *Pbam*). There is however, a set of additional reflections which can be accounted only by a further doubling of the *c*-parameter resulting in the ($\sqrt{2}a_p \times 2\sqrt{2}a_p \times 4a_p$) superstructure. This superstructure type has been reported in many $BiFeO_3$-derrived perovskites, including as prepared $BiFe_{1-y}Sc_yO_3$ compositions with $0.2 < y < 0.6$ (see Fig 1 of the main text). In all cases, the structure is orthorhombic *Pnma* with the unit cell dimension ($\sqrt{2}a_p \times 4a_p \times 2\sqrt{2}a_p$). Attempts to adopt this model to refine the structure of the annealed $BiScO_3$ were unsuccessful, resulting in a very poor fitting quality of the weak superstructure reflections (see Fig. S11). To improve the model, we systematically tested all the possible isotropy subgroups associated with the **k**=(0,0,1/2) propagation vector (Z-point of symmetry of the *Pbam* space group) against the available diffraction data. Between the eight possibilities listed in Table S6, only two structural models provide a good fitting quality. These models are related to the Z_1^+ and Z_3^+ irreducible representations of the *Pbam* space group and they have *Pbam* ($2\sqrt{2}a_p \times \sqrt{2}a_p \times 4a_p$) and *Pnma* ($2\sqrt{2}a_p \times 4a_p \times \sqrt{2}a_p$) symmetries, respectively. The refinement done in the first subgroup, however, converged with unphysically large thermal parameters for Bi and oxygen ions, whereas all the fitting parameters are meaningful in the second subgroup, indicating that this is the right model.
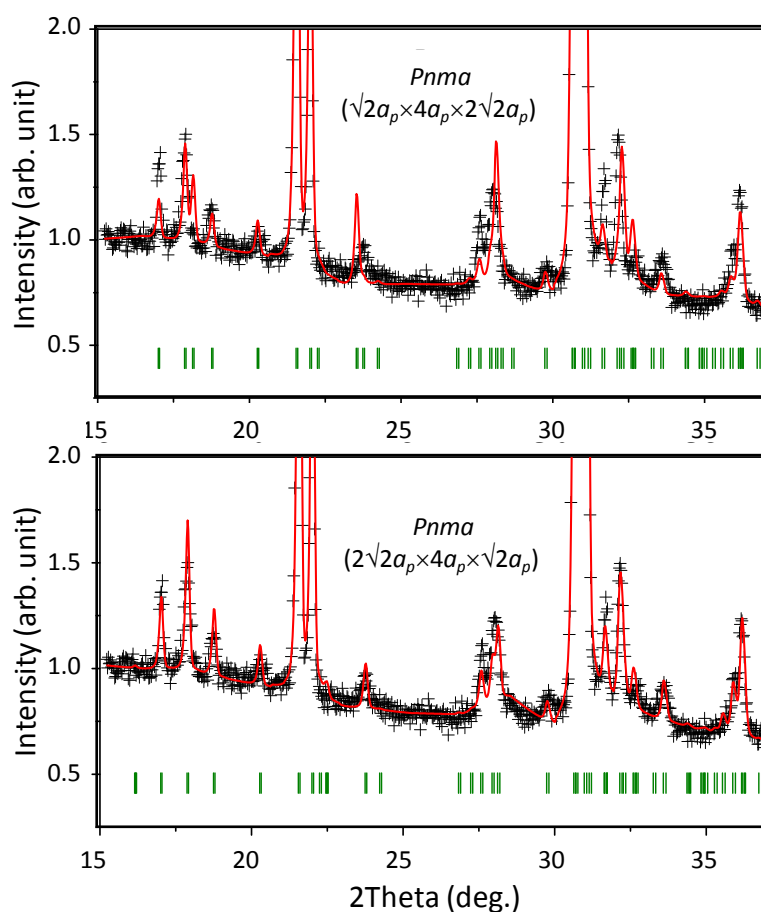
Fig. S12 Fitting quality of the superstructure reflections of the X-ray diffraction pattern collected for the annealed $BiScO_3$ sample at room temperature in different models.

Table S6 Reliability factors for the refinements of the neutron diffraction data collected for the annealed BiScO$_3$ sample in the different isotropy subgroups of the *Pbam* space group, associated with the k=(0,0,1/2) propagation vector.

Space group	Irrep	Basis	Origin	R$_{Bragg}$(%)	R$_P$(%)	R$_{wp}$(%)
Pbam	Z$_1^+$	(1,0,0)(0,1,0)(0,0,2)	(0,0,0)	7.07	6.17	6.71
Pnnm	Z$_2^+$	(1,0,0)(0,1,0)(0,0,2)	(0,0,0)	8.33	7.15	8.36
Pnma	**Z$_3^+$**	**(0,1,0),(0,0,2),(1,0,0)**	**(0,0,0)**	**6.10**	**5.93**	**6.39**
Pnma	Z$_4^+$	(1,0,0)(0,0,2)(0,-1,0)	(0,0,0)	7.38	6.96	8.10
Pnnm	Z$_1^-$	(1,0,0)(0,1,0)(0,0,2)	(0,0,1/2)	10.8	7.39	8.45
Pbam	Z$_2^-$	(1,0,0)(0,1,0)(0,0,2)	(0,0,1/2)	9.80	6.63	7.23
Pnma	Z$_3^-$	(1,0,0)(0,0,2)(0,-1,0)	(0,0,1/2)	10.8	7.46	9.11
Pnma	Z$_4^-$	(0,1,0)(0,0,2)(1,0,0)	(0,0,1/2)	8.53	6.46	7.05

Table S7. Atomic coordinates and thermal parameters for the conversion-stabilized orthorhombic polymorph BiScO$_3$ at *T*=300 K, refined in the *Pnma* space group with the basis vectors related to the parent cubic cell as a_o=2a_p-2c_p, b_o=4b_p, c_o=a_p+c_p and origin at (a_p/2+b_p/2). Unit cell parameters: a_o=11.6769(5)Å, b_o=16.1629(3)Å and c_o=5.8244(2)Å. R$_{Bragg(X-ray)}$=5.40%, R$_{Bragg(neutr)}$=6.10%

Atom	Site	x	y	z	B
Bi1	8*d*	0.8649(9)	-0.0003(7)	0.308(1)	1.8(1)
Bi2	4*c*	0.872(1)	0.25000	0.330(2)	1.8(1)
Bi3	4*c*	0.612(1)	0.25000	0.692(2)	1.8(1)
Sc1	8*d*	0.8789(9)	0.8779(6)	0.7518(8)	2.38(7)
Sc2	8*d*	0.8716(9)	0.3733(5)	0.7455(7)	2.38(7)
O1	8*d*	-0.010(1)	0.8560(6)	0.034(2)	1.9(1)
O2	8*d*	0.520(1)	0.8478(8)	-0.041(2)	1.9(1)
O3	8*d*	0.253(1)	0.9071(5)	0.506(3)	1.9(1)
O4	8*d*	0.235(1)	0.4033(6)	0.513(3)	1.9(1)
O5	8*d*	0.920(1)	0.0074(8)	0.709(2)	1.9(1)
O6	4*c*	0.824(2)	0.25000	0.677(3)	1.9(1)
O7	4*c*	0.674(2)	0.25000	0.306(2)	1.9(1)

Table S8. Decomposition of the *Pnma* structure of BiScO₃ in respect of the symmetrized displacive modes of the parent cubic $Pm\bar{3}m$ perovskite structure (a_p=4.09568Å, Bi 1*b*(1/2,1/2,1/2), Fe/Sc 1*a*(0,0,0) and O 3*d(*1/2,0,0)). The column "Irrep (***k***)" shows the irreducible representation of the $Pm\bar{3}m$ space group and the arms of the wave vector star involved (for the propagation vectors inside the Brillouin zone, −***k*** are not displayed). The column "Order parameter" lists the projections of the reducible order parameter onto the corresponding irreducible subspace (the same symbol in different positions indicates equal order parameter components). The column "Amplitude" displays amplitudes (in Å) of the displacive modes. The column "Site irrep" shows the corresponding point-group symmetry irrep of the local Wyckoff position and the order parameter component (in brackets).

Irrep (***k***)	Order parameter	Site irrep	Amplitude
	Strains		
Γ_1^+ (0,0,0)	(*a*), $e_{xx}+e_{yy}+e_{zz}$	(*a*)	0.00008
Γ_3^+ (0,0,0)	(*a*,−√3*a*), -e_{xx}-e_{zz}+2e_{yy}	(*a*)	-0.01649
Γ_5^+ (0,0,0)	(0,0,*a*), e_{xz}	(*a*)	-0.00172
	Bi-displacement		
Δ_5 (0,1/4,0)	(0,*a*,-*a*,0;0,0,0,0;0,0,0,0)	T₁ᵤ(*a*)	-0.22772
Λ_3 (-1/4,1/4,1/4), (1/4,1/4,-1/4)	(0,0,0,0;*a*,-*a*,√3*a*,√3*a*;0,0,0,0;-√3*a*,-√3*a*,*a*,-*a*)	T₁ᵤ(*a*)	1.18775
Σ_2 (1/4,0,-1/4)	(0,0;0,0;0,0;*a*,-*a*;0,0;0,0)	T₁ᵤ(*a*)	0.73908
R_5^+ (1/2,1/2,1/2)	(*a*,-*a*,0)	T₁ᵤ(*a*)	0.40198
M_5^- (1/2,0,1/2)	(0,0;*a*,-*a*;0,0)	T₁ᵤ(*a*)	-0.00116
S₄ (1/4,1/2,-1/4)	(0,0;*a*,-*a*;0,0;0,0;0,0;0,0)	T₁ᵤ(*a*)	0.56532
T₃ (1/2,1/4,1/2)	(0,0;*a*,-*a*;0,0)	T₁ᵤ(*a*)	-0.01853
	Sc-displacement		
Δ_5 (0,1/4,0)	(0,*a*,-*a*,0;0,0,0,0;0,0,0,0)	T₁ᵤ(*a*)	0.12048
Λ_3 (-1/4,1/4,1/4), (1/4,1/4,-1/4)	(0,0,0,0;*a*,-*a*,√3*a*,√3*a*;0,0,0,0;-√3*a*,-√3*a*,*a*,-*a*)	T₁ᵤ(*a*)	0.04286
Σ_2 (1/4,0,-1/4)	(0,0;0,0;0,0;*a*,-*a*;0,0;0,0)	T₁ᵤ(*a*)	-0.00579
X_3^- (0,1/2,0)	(*a*;0;0)	T₁ᵤ(*a*)	-0.11107
M_5^- (1/2,0,1/2)	(0,0;*a*,-*a*;0,0)	T₁ᵤ(*a*)	-0.0509
	O-displacement		
Δ_5 (0,1/4,0)	(0,*a*,-*a*,0;0,0,0,0;0,0,0,0)	A₂ᵤ(*a*)	0.11758
		Eᵤ(*a*)	-0.21141
		Eᵤ(*a*)	0.18021
Λ_2 (-1/4,1/4,1/4), (1/4,1/4,-1/4)	(0,0;0,*a*;0,0;-*a*,0)	Eᵤ(*a*)	-0.10073
			-0.17166
Λ_3 (-1/4,1/4,1/4), (1/4,1/4,-1/4)	(0,0,0,0;*a*,-*a*,√3*a*,√3*a*;0,0,0,0;-√3*a*,-√3*a*,*a*,-*a*)	A₂ᵤ(*a*)	0.22199
		Eᵤ(*a*)	1.23297
		Eᵤ(*a*)	-0.91690
Σ_2 (1/4,0,-1/4)	(0,0;0,0;0,0;*a*,-*a*;0,0;0,0)	A₂ᵤ(*a*)	0.02457
		Eᵤ(*a*)	0.59797
		Eᵤ(*a*)	-0.54099
R_4^+ (1/2,1/2,1/2)	(*a*,*a*,0)	Eᵤ(*a*)	-3.27491
R_5^+ (1/2,1/2,1/2)	(*a*,-*a*,0)	Eᵤ(*a*)	0.40198
X_3^- (0,1/2,0)	(*a*;0;0)	Eᵤ(*a*)	-0.17145
M_5^- (1/2,0,1/2)	(0,0;*a*,-*a*;0,0)	Eᵤ(*a*)	0.13206
S₄ (1/4,1/2,-1/4)	(0,0;*a*,-*a*;0,0;0,0;0,0;0,0)	Eᵤ(*a*)	-0.46527
		Eᵤ(*a*)	0.42514
T₁ (1/2,1/4,1/2)	(0,0;*a*,*a*;0,0)	A₂ᵤ(*a*)	-0.28324

		A$_{2u}$(a)	0.29656
T$_3$ (1/2,1/4,1/2)	(0,0;a,-a;0,0)	E$_u$(a)	-0.16624

Density functional calculations for structure verification of the orthorhombic Pnma polymorph To further verify the structural model of BiScO$_3$ obtained experimentally, a set of *ab initio* density functional calculations (DFT) has been performed. The total energy of different structural models listed in Table S3 was evaluated with experimental and relaxed atomic coordinates and unit cell parameters. The calculations were done by using plane-wave pseudo-potential method implemented in open-source QUANTUM ESPRESSO[8] package. For exchange-correlation functional Perdew–Burke–Ernzerhof (PBE)[9] generalized gradient approximation (GGA) was employed. Projector augmented wave (PAW) pseudopotentials were applied. Using the experimentally obtained structural parameters, total energies were calculated as a function of volume of the unit cell, and were fitted to the Murnaghan equation. The total energy at the theoretical values of equilibrium lattice parameters and relative difference of the unit cell volume in comparison with the experimental one are shown below in Table S6. It can be seen that the minimum of total energy corresponds to the *Pnma* (Z_3^+) model. The same is valid for the cases when the unit cell parameters and atomic coordinates were allowed to relax and the relaxation was successful.

Table S9 Total energy for different structural models of BiScO$_3$ calculated using the experimental unit cell and atomic coordinates and relaxed ones for the cases when the relaxation converged successfully. The change of the unit cell volume in comparison with the experimental one (ΔV) after relaxation, are provided as well.

Space group	Irrep	Total energy at experimental volume per f.u. (Ry)	Total energy at theoretical volume per f.u. (Ry)	ΔV (%)	Total energy after structural relaxation per f.u. (Ry)	ΔV (%)
Pbam	Z_1^+	−1188.7212	−1188.7231	2.9	−1188.74552	1.1
Pnnm	Z_2^+	−1177.7770				
Pnma	Z_3^+	**−1188.7352**	**−1188.7373**	**3.0**	**−1188.7532**	**2.8**
Pnma	Z_4^+	−1188.6252	−1188.6313	5.3		
Pnnm	Z_1^-	−1187.2708	−1187.5756	52.8		
Pbam	Z_2^-	−1188.7144	−1188.7152	1.9		
Pnma	Z_3^-	−1188.5929	−1188.6002	5.8		
Pnma	Z_4^-	−1188.6966	−1188.6988	3.1		

References

[1] A. N. Salak, D. D. Khalyavin, A. V. Pushkarev, Yu. V. Radyush, N. M. Olekhnovich, A. D. Shilin, V. V. Rubanik, *J. Solid State Chem.*, 2017, **247**, 90.

[2] L. C. Chapon, P. Manuel, P. G. Radaelli, C. Benson, L. Perrott, S. Ansell, N. J. Rhodes, D. Raspino, D. Duxbury, E. Spill, and J. Norris, *Neutron News*, 2011, **22**, 22.

[3] J. Rodriguez Carvajal, Physica B, 1993, **192**, 55.

[4] H. T. Stokes, D. M. Hatch, and B. J. Campbell, ISOTROPY Software Suite, iso.byu.edu.

[5] B. J. Campbell, H. T. Stokes, D. E. Tanner, and D. M. Hatch, *J. Appl. Crystallogr.*, 2006, **39**, 607.

[6] D. D. Khalyavin, A. N. Salak, N. M. Olekhnovich, A. V. Pushkarev, Yu. V. Radyush, P. Manuel, I. P. Raevski, M. L. Zheludkevich, M. G. S. Ferreira, *Phys. Rev. B*, 2014, **89**, 174414.

[7] A. A. Belik, S. Iikubo, K. Kodama, N. Igawa, S. Shamoto, M. Maie, T. Nagai, Y. Matsui, S. Yu. Stefanovich, B. I. Lazoryak, and E. Takayama-Muromachi, J. Am. Chem. Soc. 2006, **128**, 706.

[8] P. Giannozzi *et al*, *J. Phys.: Condens. Matter* **2009**, 21, 395502.

[9] J. P. Perdew, K. Burke, and M. Ernzerhof, *Phys. Rev. Lett.* **1997**, 78, 1396.